Structural Organization of the Cell Wall of Halophilic Fungi

Liyanage D. Fernando[1], Yordanis Pérez-Llano[2], Malitha C. Dickwella Widanage[1$], Liliana Martínez-Ávila[2], Andrew S. Lipton[3], Nina Gunde-Cimerman[4], Jean-Paul Latgé[5,6], Ramón Alberto Batista-García[2,*], Tuo Wang[1,*]

[1] Department of Chemistry, Michigan State University, East Lansing, MI, USA
[2] Centro de Investigación en Dinámica Celular, Instituto de Investigación en Ciencias Básicas y Aplicadas, Universidad Autónoma del Estado de Morelos, Cuernavaca, Mexico
[3] Environmental Molecular Sciences Laboratory, Pacific Northwest National Laboratory, Richland, WA, USA
[4] Department of Biology, University of Ljubljana, Ljubljana, Slovenia
[5] Institute of Molecular Biology and Biotechnology, University of Crete, Heraklion, Greece
[6] Fungal Respiratory Infections Research Unit and SFR ICAT, University of Angers, France

[$]Current address: Department of Chemistry, University of Michigan, Ann Arbor, MI 48109, USA

*Correspondence: wangtuo1@msu.edu; rabg@uaem.mx

ABSTRACT

Halophilic fungi, which thrive in hypersaline habitats and face a range of extreme conditions, have gained considerable attention for their potential applications in harsh industrial processes. However, the role of the cell wall in surviving these environmental conditions remains unclear. Here we employ solid-state NMR spectroscopy to compare the cell wall architecture of *Aspergillus sydowii* and other halophilic and halotolerant fungi across salinity gradients. Analyses of intact cells reveal that *A. sydowii* cell walls contain a rigid core comprising chitin, β-glucan, and chitosan, shielded by a surface shell composed of galactomannan and galactosaminogalactan. When exposed to hypersaline conditions, *A. sydowii* enhances chitin biosynthesis and incorporates α-glucan to create thick, stiff, and hydrophobic cell walls. Such structural rearrangements enable the fungus to adapt to both hypersaline and salt-deprived conditions, providing a robust mechanism for withstanding external stress. These molecular principles can aid in the optimization of halophilic strains for biotechnology applications.

INTRODUCTION

Extremophiles are organisms that survive and thrive in harsh environments characterized by unfavorable temperature, pressure, acidity, and salinity[1,2]. Understanding their adaptation strategies can gain insights into the origin of life under extreme conditions and provide solutions to geo-ecological challenges[3-5]. Halophilic and halotolerant fungi inhabit hypersaline habitats and have shown their potential in various industrial applications, such as contaminant treatment of saline wastewater, fermentation-based production of high-value molecules and pharmaceuticals, and biofuel production[6-8]. Halophilic fungi also hold promise as a source of transgenes encoding for salt-tolerant proteins to enhance the halotolerance of other organisms[7,9]. These applications have not reached their full potential due to our incomplete understanding of adaptation mechanisms.

When exposed to hypersaline environment, fungi need to maintain positive cell turgor pressure. This requires a multitude of cellular processes, including the accumulation of compatible organic solutes, modification of cell membrane composition and fluidity, pigment production, ion homeostasis, as well as cell wall remodeling[10,11]. These physiological responses involve changes in gene expression profiles to provide osmotic balance, oxidative stress management, and metabolic rewiring of the fungal cells[11,12]. Morphological changes have also been observed in the cell walls of the model basidiomycetous halophile *Wallemia ichthyophaga* and the extremely halotolerant black yeast *Hortaea werneckii*[10]. With high salinity, *W. ichthyophaga*

produced three-fold thickened cell walls and bulky multicellular clumps while *H. werneckii* showed compromised cell wall integrity when melanin synthesis was inhibited[13-15]. Nevertheless, the ultrastructural change of the cell wall is yet to be explored.

Many *Aspergillus* species, such as *A. niger, A. flavus, A. tubingensis, A. atacamensis, A. destruens, A. versicolor*, and more recently *A. sydowii*, have been examined to understand their growth at high NaCl concentrations[16,17]. *A. sydowii* is an ascomycetous filamentous fungus found in various habitats, including salterns, dried food, decaying plant matter, and sea water, where it is a major contributor to coral disease aspergillosis[18]. Recent transcriptomic and imaging studies of *A. sydowii* revealed that under high salt concentration (2 M NaCl), there were significant changes in gene expression related to cell wall biogenesis, which led to a significant thickening of the mycelial cell wall[16]. The upregulation of hydrophobin genes further supports the role of these proteins in cell wall haloadaptation. While these findings indicate that the thickness, composition, and architecture of the cell wall are crucial for fungal survival, characterizing such changes is challenging due to the heterogeneity and insolubility of this organelle.

Recently, the use of solid-state NMR (ssNMR) spectroscopy has led to a better understanding of the molecular architecture and dynamics of fungal cell walls[19-22]. Through integrated ssNMR and biochemical analyses of *Aspergillus fumigatus*, it has been discovered that a poorly hydrated, mechanically stiff core is formed by physically associated chitin and α-1,3-glucan[23-25], which is conserved in both mycelia and conidia[26], but with altered molecular composition during morphotype transition[27]. Highly branched β-1,3/1,6-glucans and linear terminal threads of β-1,3/1,4-glucans comprise the mobile and well-hydrated meshes. The inner domain is shielded by a dynamic outer layer that contains galactomannan (GM), galactosaminogalactan (GAG), α-1,3-glucan, and protein components[24]. By directly using intact fungal cells, the need for chemical extraction and solubilization procedures has been eliminated. The physical profiles of biopolymers observed through ssNMR, such as dynamics and hydrophobicity, naturally complement the chemical solubility, linkage pattern, and localization of carbohydrates investigated by chemical assays and imaging techniques[28-31], which allow for a complete portrait of the cell wall organization to be assembled[19].

In this study, we employ high-resolution ssNMR to examine uniformly ^{13}C, ^{15}N-labeled *A. sydowii* cells cultured at different salt concentrations. Under optimal salt concentration, the cell

wall in *A. sydowii* exhibits an interlaced structure like that of *A. fumigatus* but with the addition of chitosan and the exclusion of α-1,3-glucan. These characteristics were repeatedly observed in other halophilic *Aspergillus* species. The amount of chitin and the proportion of amino sugars in GAG progressively increases as the salt concentration rises, with a small amount of α-1,3-glucan reintroduced to the mobile phase at hypersaline conditions. Chitosan and β-glucans are tightly associated with chitin and each other, but a high concentration of salt weakens these packing interactions and promotes the self-aggregation of biomolecules. These structural adjustments allow *A. sydowii* to produce thick and rigid cell walls with limited water permeability. The dehydration and rigidification of protein and lipid components further contribute to this effect. These molecular-level modifications in the fungal cell walls and associated organelles help the microorganisms maintain the structural integrity of their carbohydrate frame and lower water potential than their surroundings.

RESULTS

Structural complexity of *A. sydowii* carbohydrates

Variations in the structural organization of the fungal cell wall are often associated with the change in the environment[32]. We used *A. sydowii* as a halophile model and characterized its mycelia grown without and with NaCl at two different concentrations: optimal salinity (0.5 M) and hypersaline condition (2.0 M). The cell wall of *A. sydowii* grown at the optimal salt concentration of 0.5 M is a composite of biopolymers with distinct mobilities. We found that the rigid polysaccharides included chitin, β-1,3-glucan, and chitosan (**Fig. 1a**), while the mobile fraction mainly contained β-1,3-glucans, GM, and GAG (**Fig. 1b**). Rigid molecules were selectively detected using a two-dimensional (2D) ^{13}C-^{13}C correlation spectrum that relied on dipolar-based ^{1}H-^{13}C cross-polarization (CP) for creating the initial magnetization (**Fig. 1c**). The spectrum was dominated by the signals of chitin and β-1,3-glucan, such as the characteristic C1-C2 cross peak of chitin at (103.6, 55.5 ppm) and the C1-C3 cross peak of β-1,3-glucan at (103.6, 86.4 ppm). Chitosan, a deacetylated form of chitin, was also detectable, though relatively weak. These three types of polysaccharides form rigid scaffolds that share the mechanical load of the polymer network in the mycelial cell wall.

Mobile polysaccharides were detected by a combination of ^{13}C direct polarization (DP) and a short recycle delay of 2 s in the 2D refocused *J*-INADEQUATE[33] spectrum (**Fig. 1d**). This technique filtered out rigid molecules with slow ^{13}C-T_1 relaxation. The spectrum showed well-dispersed signals of galactose (Gal), galactosamine (GalN), and N-acetylgalactosamine

(GalNAc), which combine to form the heteroglycan GAG found on cell surfaces[34]. We also identified signals of 1,2- and 1,6-linked α-mannose ($Mn^{1,2}$ and $Mn^{1,6}$), which make up the backbone of GM, and the galactofuranose (Gal*f*) residues that form GM sidechains[35,36].

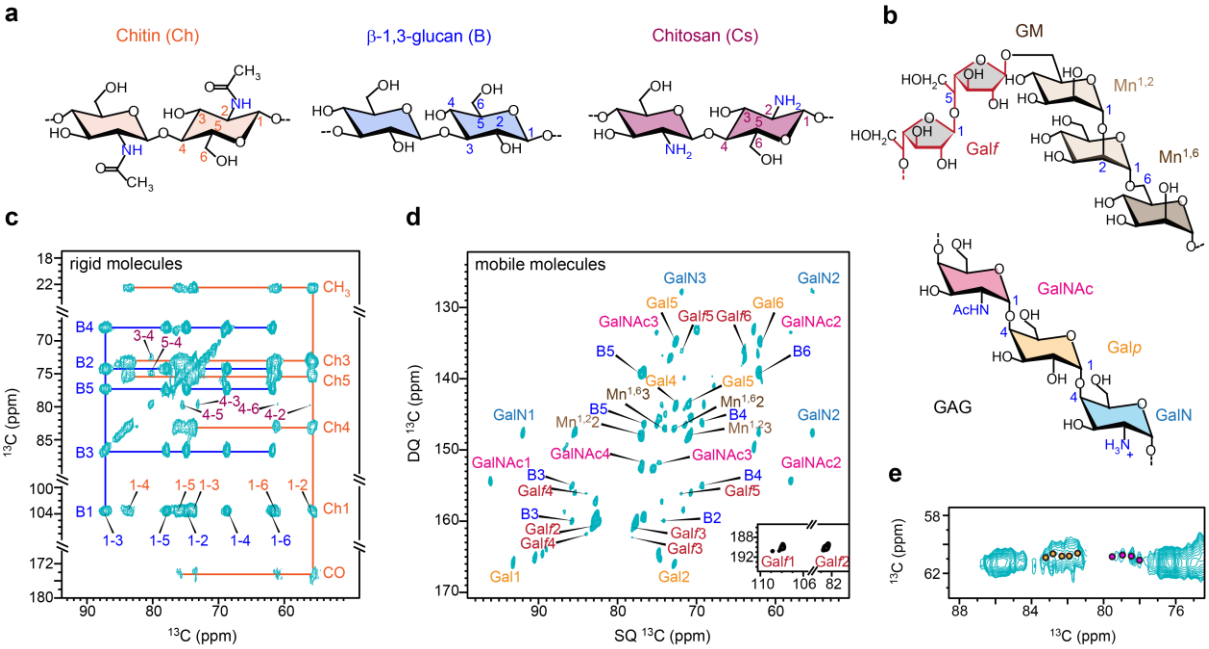

Figure 1. Rigid and mobile polysaccharides of *A. sydowii*. a, Simplified structural presentation of rigid polysaccharide in the cell wall. Carbon numbers and the NMR abbreviations are given for each polysaccharide. **b,** Representative structures of GAG and GM in the mobile domain, with key sugar units labeled. **c,** 2D ^{13}C-^{13}C correlation spectrum of *A. sydowii* measured with CP and 100 ms DARR detecting rigid molecules. Orange and blue solid lines trace the carbon linkages of chitin and β-1,3-glucan, respectively. Each cross peak is the correlation of two carbons, such as the 1-4 cross peak in orange, which represents the correlation between carbons 1 and 4 of chitin. **d,** ^{13}C DP refocused *J*-INADEQUATE spectrum detecting mobile polysaccharides. Assignments contain NMR abbreviation and carbon number, for example, B5 represents β-1,3-glucan carbon 5. **e,** Ch6-4 region of 2D ^{13}C-^{13}C correlation spectrum resolving five chitin forms (orange circles) and four chitosan types (magenta circles). All spectra were measured on an 850 MHz NMR spectrometer at 13 kHz MAS on intact *A. sydowii* cells grown with 0.5 M NaCl.

Although GM and chitin have been found to be covalently bridged through β-1,3-glucan as an integrated structural domain[28], our results identified these two molecules in two dynamically distinct fractions. This can result from the distribution of β-1,3-glucan in both rigid and mobile domains (**Fig. 1c, d**), where it experiences a transition from the rigid side that is bridged to stiff chitin to a mobile end that is connected to dynamic GM. The GM-β-1,3-glucan-chitin complex accommodates a broad gradient of dynamics. It is also possible that this covalently linked complex may only have a low population, resulting in the observed dynamics being predominantly governed by the individual polysaccharides that exist separately in the bulk.

Polysaccharides are inherently polymeric when placed in the cellular environment. Five chitin forms and four chitosan forms were identified as clustered signals (**Fig. 1e**), indicating a small range of structural variation within each molecule, probably by conformational distribution and H-bonding difference. The chemical shifts of these chitin molecules resembled those of the α-type model with antiparallel chain packing in the crystallite, while chitosan aligned with a non-flat, relaxed two-fold helix structure (called type-II chitosan) as recently reported[37]. These structural allomorphs, as well as the cell structural fingerprints, were fully retained across different halophilic *Aspergillus* species (**Supplementary Fig. 1**).

Influence of NaCl environment on *A. sydowii* carbohydrate profile

The ultrastructure of the *A. sydowii* cell wall was examined using transmission electron microscopy (TEM) (**Supplementary Fig. 2**). The thickness of the cell wall was 140 nm ± 30 nm under the optimal culture condition of 0.5 M NaCl but increased to 200 ± 20 nm at hypersaline conditions, respectively (**Fig. 2a**). The ratio between the cell wall thickness and the total mycelial cell width was found to increase with the increasing concentration of salt in the medium. Under osmotic stress, the stiff carbohydrate core effectively retained its structural integrity. We observed generally consistent patterns in the polysaccharide region when comparing samples cultured at varying salt concentrations, while significant differences were exhibited by proteins and lipids (**Fig. 2b**). Chitin signals were initially weak in the sample lacking NaCl but became stronger in the presence of NaCl (**Fig. 2c**). Quantification of peak volumes revealed an upsurge in the chitin content with increasing salinity, while the amount of hydrophilic β-glucan decreased gradually (**Fig. 2d** and **Supplementary Table 1**). The introduction of more crystalline chitin to the cell wall inevitably strengthened this biomaterial.

As salt concentration increased, the amount of GM dropped substantially but the amount of GAG increased slightly (**Fig. 2d, e**). Surprisingly, we also observed a low amount of mobile α-1,3-glucan in the hypersaline sample, but not in optimal or salt-free conditions (**Fig. 2f** and **Supplementary Fig. 3**). Under the hypersaline condition, the contents of amino sugars, including GalNAc and GalN, were doubled compared to fungal cultures under normal and low salt conditions (**Fig. 2d**). The slightly acidic pH of *A. sydowii* culture is well below the GalN pKa of ~11.8; therefore, GalN favorably occurs as $GalNH_3^+$ (**Fig. 1b**) rather than as the conjugate base $GalNH_2$. The enrichment of GalN units should have modified the physicochemical properties of GAG and made it more cationic. This is crucial for facilitating

its adherence to anionic surfaces, including human cells, and promoting the adhesion between mycelia, which helps the entire colony withstand unfavorable conditions[38,39].

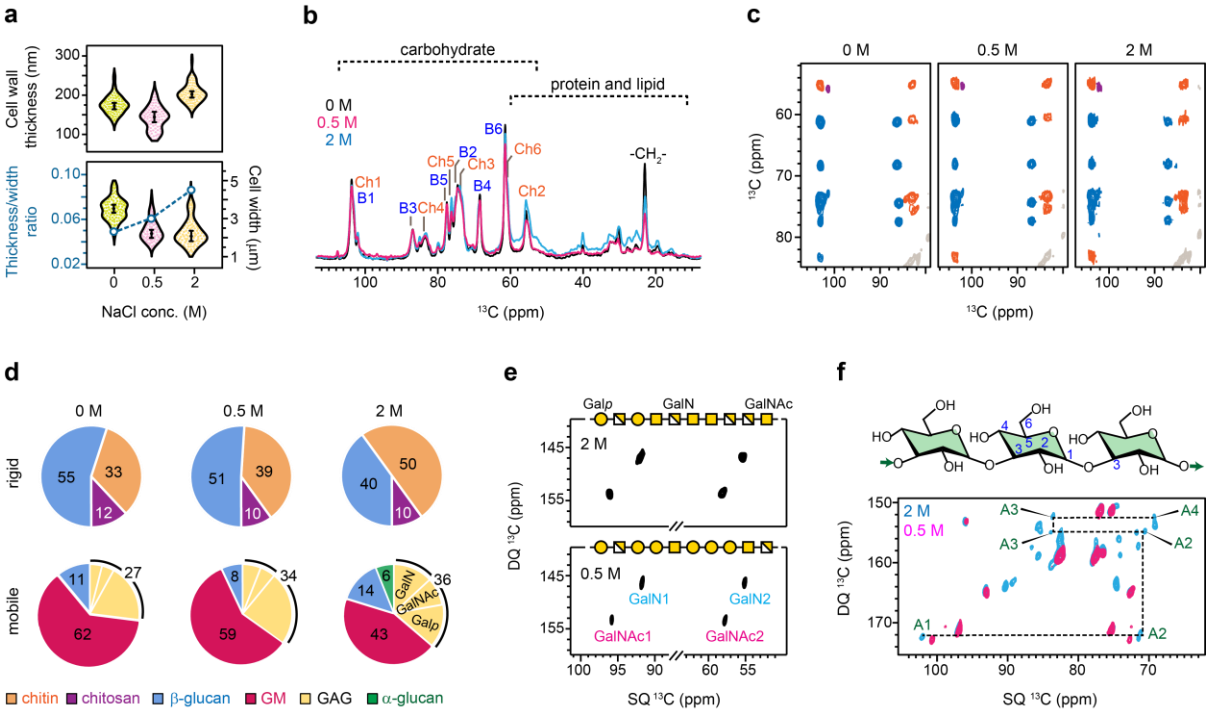

Figure 2. Effect of salt concentration on *A. sydowii* polysaccharide composition. a, Distribution of cell wall thickness (top panel) and its relative ratio to the cell thickness (bottom panel) in *A. sydowii* hyphae exposed to different NaCl concentrations. Each violin plot of cell wall thickness depicts 100 measurements from 10 cells (n=100), with the average value and standard deviation presented. The ratios of cell wall thickness to cell width were shown using blue open circles and connected by dashlines (left axis) while the violin plots of cell width values are projected to the right axis. n=100 (10 cells) for either the 0 M or 2 M sample and n=70 (7 cells) for the 0.5 M sample. **b,** Comparison of 1D ^{13}C CP spectra of *A. sydowii* cultures at 0 M, 0.5 M and 2.0 M NaCl. Key features of carbohydrate and protein/lipid signals are labeled for chitin (Ch), β-1,3-glucan (B) and the CH_2 of lipid acyl chain. **c,** 2D ^{13}C-^{13}C DARR correlation spectra of *A. sydowii* samples, with chitin signals (orange), β-1,3-glucan signals (blue), and chitosan (purple) signals marked. The relative abundance of chitin increases at high salt concentrations. **d,** Molar composition of the rigid (top row) and mobile (bottom row) polysaccharides in *A. sydowii* cell walls, determined by peak volumes of 2D ^{13}C CP DARR and ^{13}C DP *J*-INADEQUATE spectra, respectively. The fractions of Gal*p*, GalN, and GalNAc in GAG are also shown. **e,** Stronger signals of GalN and GalNAc units in GAG at the higher salt concentration in ^{13}C DP *J*-INADEQUATE spectra. GAG structures are constructed following the molar fraction using the Symbol Nomenclature for Glycans. **f,** Structure of α-1,3-glucan (A) and carbon connectivity tracked by ^{13}C DP *J*-INADEQUATE spectra. α-1,3-glucan is barely detectable in 0.5 M NaCl condition but becomes visible in 2.0 M NaCl condition. Source data of Figs. 2a, d are provided as a Source Data file.

Remodeled polymer network of the cell wall

The mechanical properties and nanoscale assembly of cell walls are governed by the intermolecular interactions of biomolecules[40]. Sub-nanometer polymer contacts were identified

through a 2D ^{13}C-^{13}C correlation measured with a 1.5 s proton-driven spin diffusion (PDSD) mixing period. For example, many cross-peaks were unambiguously identified between chitin methyl groups and chitosan carbons (**Fig. 3a**). However, some cross-peaks observed at optimal conditions, such as the chitin carbon 4 and chitosan carbon 1 (Ch4-Cs1) and between β-1,3-glucan carbon 3 and chitosan carbon 4 (B3-Cs4) observed in **Fig. 3a**, disappeared in the hypersaline sample (**Supplementary Fig. 4**), suggesting loosened packing interfaces between chitosan and chitin/glucan at hypersaline condition.

Analysis of 30 intermolecular cross peaks uncovered the organization pattern of the polysaccharide network (**Supplementary Table 2**). The interactions between different carbon-4 sites of chitin units revealed the coexistence of these sub-forms in the same chitin crystallite (**Fig. 3b**). This is a conserved feature found in both 0.5 M and 2.0 M *A. sydowii* samples. Crystalline chitin is physically supported by the β-glucan matrix and can also covalently link to β-glucan and then to GM, as reported by NMR and chemical assays of *A. fumigatus*[24,28]. Although the semi-dynamic β-glucan was disfavored in long-range correlation experiments, its carbon 3 and carbon 5 still showed strong cross peaks with the carbon 5 and methyl of chitin, regardless of the salt concentration. Under optimum salt concentration, chitosan was mixed with both chitin and β-glucan, but such contacts became limited in the hypersaline habitat. The hyperosmotic condition induced the restructuring of fungal cell walls.

Changes in water accessibility and polymer dynamics

The fungal cell wall has dramatically modified its water accessibility and polysaccharide dynamics in response to varying salt concentrations. Water accessibility refers to the number of immobilized water molecules present at each carbon site, while polysaccharide dynamics pertain to the movement of these molecules on the nanosecond and microsecond timescales. Polymer hydration was investigated in a site-specific manner using a 2D ^{13}C-^{13}C correlation water-edited experiment that only detects the signals of water-associated biomolecules (**Supplementary Fig. 5**)[41,42]. The intensity of the water-edited signals (S) was compared to the equilibrium condition (S_0) to determine the S/S_0 ratio for each carbon site, which is an indicator of water retention (**Supplementary Table 3**). Such intensities were substantially higher for β-glucan than for chitin within each *A. sydowii* sample (**Fig. 3c**), which confirmed the different structural roles of these polysaccharides as recently observed in other *Aspergillus* species: chitin constitutes the hydrophobic center, while β-glucans form the hydrated matrix[23].

A. sydowii cell walls were found to be best hydrated at the optimal concentration of 0.5 M NaCl (**Fig. 3c**). Specifically, the average S/S_0 ratios for β-glucans and chitin are 0.51 for and 0.20. respectively. However, the extent of water association dropped substantially at 0 M and 2 M NaCl concentrations, both of which are considered stress conditions for *A. sydowii*. In the absence of NaCl, the hydration level of chitin remained unchanged but the S/S_0 ratio of β-glucan dropped by more than one-third. Under hypersaline conditions, both chitin and β-glucan were poorly hydrated, with S/S_0 ratios of 0.18 and 0.39, respectively.

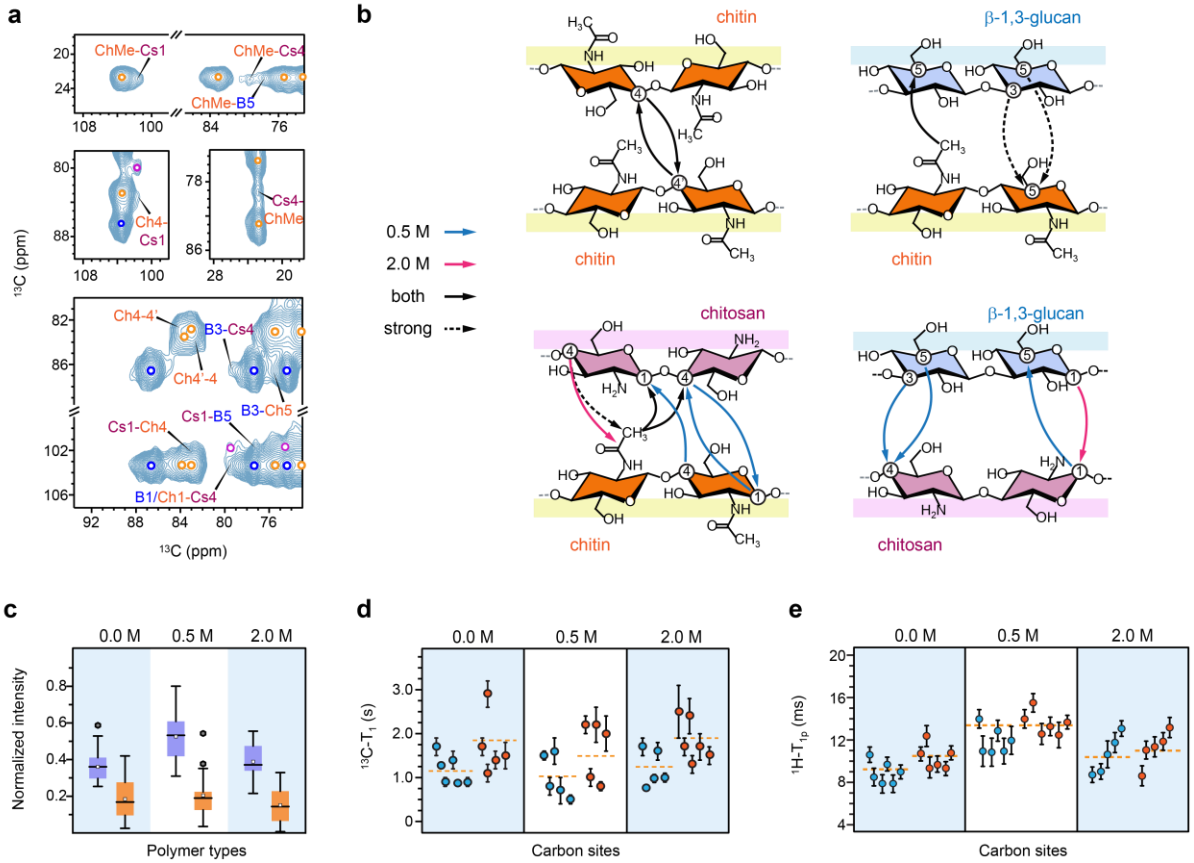

Figure 3. Packing, hydration, and dynamics of *A. sydowii* polysaccharides. a, Intermolecular cross peaks identified in 2D ^{13}C correlation spectra measured with long (1.5 s PDSD) mixing periods on 0.5 M sample. Signals of chitin (orange), β-glucan (blue) and chitosan (purple) are marked by open circles. Intermolecular peaks are labeled. **b,** Summary of intermolecular cross peaks observed in *A. sydowii*. Arrows show the direction of polarization transfer. Blue and magenta lines show the interactions observed only in 0.5 M and 2.0 M conditions, respectively. Black solid lines and dash lines represent interactions observed in both samples in both 1.5 s PDSD and 0.1 s PDSD spectra, respectively. **c**, Box-and-whisker diagram plotting the relative intensities (S/S_0) of β-1,3-glucan (blue; n=24, 25, 25) and chitin (orange; n=17, 15, 14) in three *A. sydowii* samples with varying salt concentrations. **d**, ^{13}C-T_1 relaxation time constants of β-1,3-glucan (blue) and chitin (orange) in *A. sydowii*. The average ^{13}C-T_1 are marked using yellow dash lines. **e**, ^{1}H-$T_{1\rho}$ relaxation times of β-1,3-glucan (blue) and chitin (orange). The average values over all carbon sites within a polysaccharide are shown by dash lines. For both panels e and f, error bars indicate standard deviations of the fit parameters. Source data of Figs. 3c-e are provided as a Source Data file.

The observed non-directional variations in polymer hydration cannot be easily correlated with the sequential changes in the polymer composition. The cell wall of *A. sydowii* grown in high salinity became more hydrophobic, which helps to prevent water loss from the cytoplasm. This is likely due to a lower content of β-glucans, as shown in **Fig. 2d**. However, the NaCl-free sample with a β-glucan-rich cell wall still exhibited limited exposure to water. This observation is intriguing and may be related to the increased thickness of the cell wall (**Fig. 2a**), which suggests a change in the molecular assembly of the cell wall or other associated constituents. A potential explanation is the upregulation of hydrophobin genes in *A. sydowii* samples cultured in both 2 M and 0 M NaCl concentrations, which could lead to the formation of hydrophobic protein layers[13,16].

The motional characteristics of cell wall polysaccharides were determined using NMR relaxation experiments (**Supplementary Fig. 6** and **Table 4**). A molecule with fast $^{13}C\text{-}T_1$ relaxation is highly dynamic on the nanosecond (ns) timescale, likely due to rapid local reorientation motions (**Fig. 3d**). Similarly, molecules exhibiting fast $^{1}H\text{-}T_{1\rho}$ relaxation are mobile on the microsecond (μs) time scale, typically attributed to slower collective movements and flipping (**Fig. 3e**). Within each sample, β-glucan showed shorter $^{13}C\text{-}T_1$ and $^{1}H\text{-}T_{1\rho}$ time constants than chitin, demonstrating the dynamic nature of β-glucans.

When we deviated from the optimal condition of 0.5 M to either 0 M or 2.0 M, both chitin and β-glucans showed longer $^{13}C\text{-}T_1$ (**Fig. 3d**) and shorter $^{1}H\text{-}T_{1\rho}$ (**Fig. 3e**). The average $^{13}C\text{-}T_1$ increased from 1.6 s to 1.8-2.0 s for chitin and increased from 1.0 s to around 1.2 s for β-glucan. Meanwhile, the average $^{1}H\text{-}T_{1\rho}$ dropped from 14 ms to 10-12 ms for chitin and from 12 ms to 9-10 ms for β-glucan, likely caused by the loosened interface between different polymers. Therefore, in salt-free or hypersaline environments, biopolymers in the inner cell wall have restricted reorientation motions on the nanosecond timescale but accommodate slower and larger-scale movements on the microsecond timescale. Even though the centesimal composition of the cell wall polymers is different at 0 and 2M NaCl, the biophysical data showed that polymer dynamics and hydration, as well as cell wall thickness, lead to similar changes in the cell wall assembly when deviating away from the optimal concentration.

Protein and lipid components

We observed strong signals from proteins and lipids, which could have originated from various sources, including cell walls and plasma membrane components, as well as intracellular organelles. We found that the protein and lipid components mainly reside in the mobile phase (**Supplementary Fig. 7**). The signals of amino acids were distinguished using 2D refocused *J*-INADEQUATE spectra (**Fig. 4a**). As protein backbone chemical shifts are sensitive to φ and ψ torsion angles[43], we determined the secondary structure by comparing the observed Cα chemical shifts to random-coil values. We found that mobile proteins were predominantly in α-helical conformation, which remained consistent across the salt gradient (**Fig. 4b**).

By exclusively selecting rigid molecules in structurally robust components, we noticed a distinctive and plentiful presence of proteins and lipids at 2M NaCl condition (**Fig. 2b** and **Supplementary Fig. 8**). The amino acid residues identified in this inflexible portion had a noticeable contribution to the β-strand conformation and experienced substantial dehydration in hypersaline condition (**Fig. 4c** and **Supplementary Table 5**). The rigidification and dehydration of both protein and lipid components have suggested a global change to the cell wall and its adjacent layers, including the underlying membranes and the surface hydrophobins. These spectroscopic results also support the biochemical concept that halophilic fungi increase the expression of hydrophobins to moderate surface tension and water penetration[16,44,45].

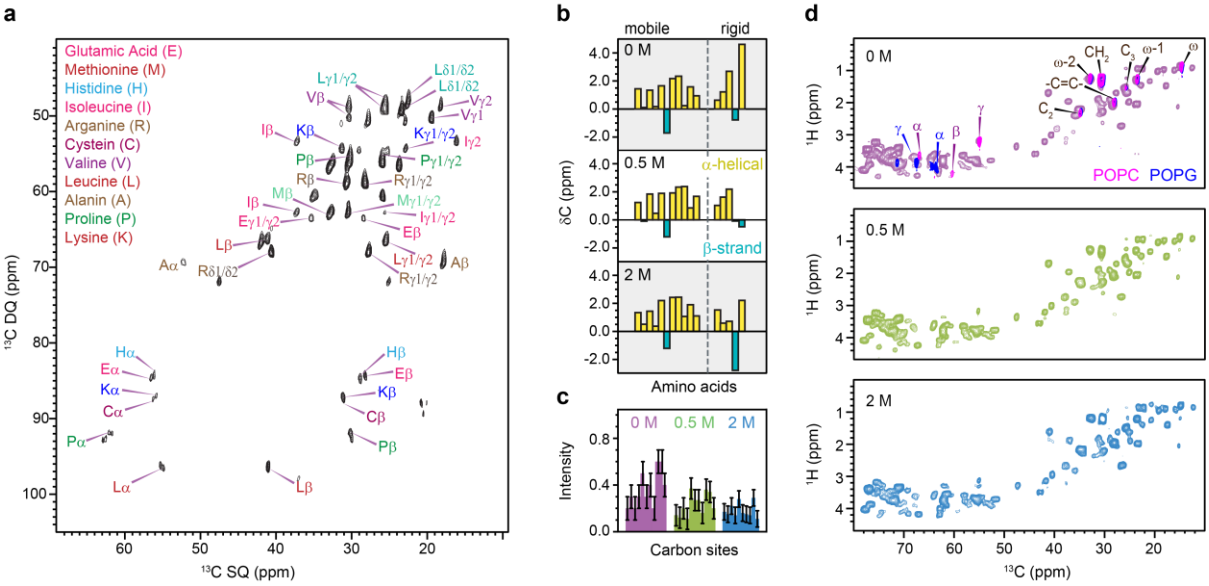

Figure 4. Fingerprints of *A. sydowii* proteins and lipids. a, Protein region of DP refocused J-INADEQUATE spectra collected using *A. sydowii* (0.5 M NaCl). **b,** Secondary structure of proteins denoted by ^{13}C chemical shifts of Cα. α-helical and β-strand conformations are in yellow and blue, respectively. The amino acid residues in the mobile fraction (left) and rigid fraction (right) are separated by dash lines. **c,** Water-edited intensities of protein carbon sites in *A. sydowii* samples cultured with

different salt concentrations. **d,** 2D refocused INEPT ^{1}H-^{13}C correlation spectra of *A. sydowii* samples cultured with 0 M, 0.5 M, and 2 M NaCl. The spectra are compared with the control spectra of model lipids POPC (magenta) and POPG (blue), showing the α, β, and γ carbons in phospholipid headgroups and the carbons in lipid tails.

The lipid components were also examined using the 2D ^{1}H-^{13}C refocused Insensitive Nuclei Enhanced by Polarization Transfer (INEPT) experiment (**Fig. 4d**)[46]. Spectral superposition of *A. sydowii* lipids and model compounds in the glycerol/headgroup region confirmed the presence of phosphatidylcholines (PC) and phosphatidylglycerols (PG) (**Supplementary Fig. 9**). Sterols and polyisoprenoids were not detectable in either mobile or rigid portion, likely due to their relatively low abundance in a cellular sample. We spotted the putative signals of triglyceride (TG), which became pronounced in 0 M and 2.0 M NaCl conditions (**Supplementary Fig. 10** and **Table 6**). This molecule has been identified in multiple *Aspergillus* and *Cryptococcus* species and was reported to modulate membrane fluidity[27,47]. However, due to the severe overlap of its putative signals with those from other lipids and proteins, and due to the broad distribution of lipid polymers in the cell, more biochemical studies should be undertaken here to explain these changes.

DISCUSSION

High-resolution solid-state NMR analysis has unveiled the molecular-level organization of *A. sydowii* cell walls. At optimum salt concentration, the inner cell wall of *A. sydowii* was found to contain rigid chitin and chitosan in partially crystalline and highly polymorphic structures[37], surrounded by a matrix mainly consisting of β-glucans that regulate the water accessibility of the cell wall mesh in the absence of α-1,3-glucan (**Fig. 5a**). Chitin and β-glucan, along with chitosan, are well mixed on the nanoscale, with extensive intermolecular interactions. This inner domain is covered by an outer shell rich in highly dynamic molecules, mainly containing GM and GAG. *Aspergillus* cell walls are characterized by covalently linked chitin-β-glucan-GM complex[28,30], which could explain the observed bimodal distribution of β-1,3-glucan in both rigid and mobile domains. The rigid segment is in contact with chitin or chitosan, while the mobile part forms the soft matrix and bridges to even more dynamic GM in the outer shell. GM and GAG should covalently connect to structural proteins through linkers formed by hydrophobic amino acid residues, as suggested by recent analyses of *A. fumigatus* cell walls[24].

To survive in hypersaline habitats with restricted water activity[17,18], halophilic fungi have to accommodate structural modifications at macroscopic and molecular levels (**Fig. 5b**). The

inner domain of the cell wall contains more chitin molecules, which provide high rigidity, and less β-1,3-glucans, which abolish water permeability. The packing interactions between chitin-chitin and chitin-glucan remain unchanged. However, chitosan becomes better isolated from other molecules, possibly due to self-aggregation. The surface layer has a reduced amount of GM but an increased content of α-1,3-glucan and GAG with an enriched fraction of deacetylated GalNAc, which supports fungal adherence and virulence[34,39,48]. The fungus develops a thickened, stiff, waterproof, and adhesive cell wall for better survival in salty conditions.

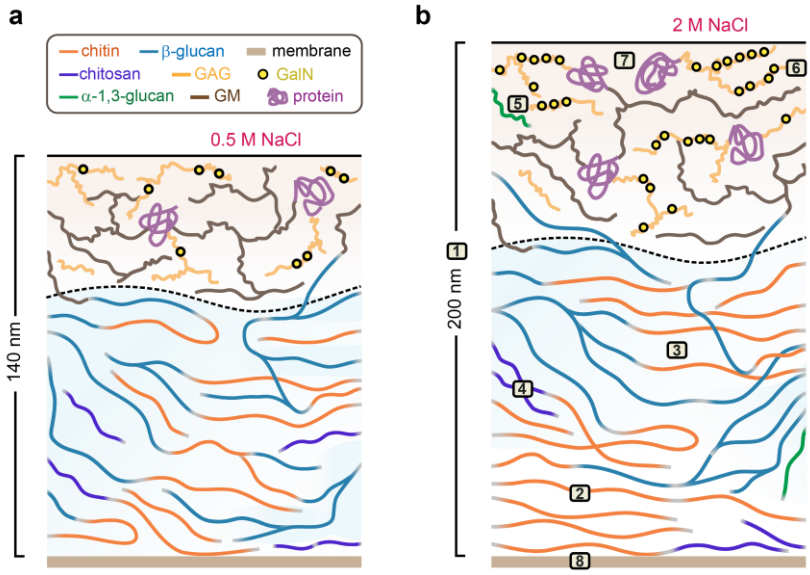

Figure 5. Schematic representation of fungal cell wall adaptation to salinity. The diagram illustrates key components of the *A. sydowii* cell walls and their distributions in the surface and inner domains separated by the dash line. The blue color gradient of the inner domain represents the extent of water retention. The cell wall thickness and the molecular composition are shown, but not strictly to scale. Compared to 0.5 M condition, the cell wall in 2.0 M NaCl exhibits 1) increased thickness, 2) enhanced biosynthesis of crystalline chitin resulting in higher cell wall rigidity and restricted local motions in the inner domain, 3) reduced water retention due to lower β-glucan content, 4) chitosan aggregation and reduced interactions with other components, 5) inclusion of α-glucan in the mobile phase, 6) enriched content of cationic GalN units in GAG on the surface, 7) increased protein content and rigidity, dehydration of protein, and reshuffled secondary structure, and 8) elevated content of rigid lipids.

In mycelia obtained under hypersaline conditions, proteins and lipids undergo a similar trend of rigidification and dehydration as observed in the cell wall polysaccharides. These effects may occur to the two layers of hydrophobins and cell membrane that sandwich the cell wall, as well as the protein and lipid components included in the macromolecular assembly of the cell wall itself. These structural changes help to constrain the cell wall permeability and better

protect the organism from the stressful environment, contributing to the adaptation of *A. sydowii* as a successful halophile.

The halophilic fungal species investigated in this study do not contain a significant amount of α-1,3-glucan (**Fig. 2c**). This finding contradicts previous observations in *A. fumigatus*, where α-1,3-glucan was found to be present in the rigid and mobile phases of the alkaline soluble and insoluble fractions[24]. This versatile molecule supports mechanical properties by interacting with chitin and enhances fungal virulence by shielding the surface[19,31,49]. The lack of α-1,3-glucan in halophilic species inevitably necessitates other molecules, such as β-glucans, to play a more prominent role in stabilizing cell wall assembly. This observation could also explain the moderate virulence of these fungal strains in pathogenicity.

It is notable that the thickened cell wall, limited water permeability, and altered motional characteristics were consistently observed in both 0 M and 2 M NaCl conditions, revealing a general mechanism of cell wall restructuring to resist external stress. This is a new paradigm in cell wall biology where similar cell wall modifications only indicate the presence of stress regardless of the nature of the stress encountered by the fungus. These molecular-level insights provide a structural vision of the osmoprotective strategies adopted by halophiles, which could inform the use of these microbes in agricultural applications and biotechnology in extreme environments[8,9].

METHODS

Microorganism and culture conditions. *A. sydowii* strain EXF-12860 was used as the primary model fungus in this study. The mycelium was routinely propagated and preserved in Potato Dextrose Agar (PDA) in the presence of 0.5 M NaCl (optimum concentration) for seven days at 28℃. For isotopic labeling, *A. sydowii* was grown in 100 mL of liquid media containing 20 g/L ^{13}C-glucose and 2 g/L ^{15}N-labeled NH_4NO_3 as labeled materials together with other salt and trace elements as detailed in **Supplementary Table 7**. The culture was grown at 28℃ with 150 rpm shaking for seven days. The fungus was grown in parallel without NaCl and with NaCl but under two different concentrations of 0.5 M (optimal) and 2.0 M (hypersalinity). The mycelium was collected and washed twice with deionized water, and later washed with PBS to remove the excess isotope-labeled molecules and NaCl. The harvested fungal mycelia were used for both solid-state NMR and TEM experiments.

To compare with the *A. sydowii* strain EXF-12860, uniformly ^{13}C,^{15}N-labeled mycelia were also obtained for other fungal species including *A. atacamensis* (EXF-6660) and *A. destruens* (EXF-10411). 20 g/L of glucose and 2 g/L of NH_4NO_3 were added to 100 mL mineral base media (**Supplementary Table 7**), which were then incubated for seven days at 28°C and 200 rpm. Each strain was exposed to two different NaCl concentrations for comparison. The optimal salt concentration was 1.0 M for *A. atacamensis* and 1.9 M (optimal) for *A. destruens*.

TEM imaging of cell wall thickness and morphology. The *A. sydowii* mycelia obtained from the three culture conditions used in this study (0 M, 0.5 M, and 2.0 M NaCl) were fixed overnight at 4 °C using 2.5% glutaraldehyde and 2 % paraformaldehyde in 0.1 M phosphate buffer (pH 7.4) to halt metabolic processes and preserve the cells. The mycelia were then embedded in 3% agarose gel and rinsed four times with 0.1 M phosphate buffer pH 7.4 and 0.05 M glycine. After washing, the samples were fixed with 2% OsO_4 in the dark for 1 h and rinsed three times using deionized water. En Bloc staining in 1% uranyl acetate was used to increase the contrast. Dehydration was achieved using 70% ethanol series and propylene oxide for two times followed by infiltration in propylene oxide:Epon resin series. Ultra-thin sections for TEM were cut on a Dupont Sorvall MT-2 microtome. TEM sections were mounted on carbon-coated copper grids (EMS FCF-150-CU) and stained with 2% uranyl acetate and Reynolds lead citrate. Measurements were performed on the perpendicular cross-sections of 100 hyphae per culture condition using a JEOL JEM-1400 (120 kV) electron microscope.

Solid-state NMR analysis of carbohydrates and proteins. For solid-state NMR analysis, 30 and 100 mg of mycelia were packed into 3.2 mm and 4 mm MAS rotors, respectively. High-resolution 1D and 2D solid-state NMR experiments were performed on a Varian VNMRS 850 MHz (19.9 Tesla) spectrometer using a 3.2 mm MAS triple-resonance HCN probe under 13 kHz MAS at 290 K. Water-editing, relaxation, and ^{1}H-^{13}C refocused INEPT experiments were conducted on a Bruker Avance 400 MHz (9.4 Tesla) spectrometer under 10 kHz MAS at 293 K. The ^{13}C chemical shifts were externally referenced to the adamantane CH_2 signal at 38.48 ppm on the tetramethylsilane (TMS) scale. The typical radiofrequency field strengths were 83 kHz for ^{1}H hard pulses and decoupling, and 50-62.5 kHz for ^{13}C pulses, unless otherwise specified. The key experimental parameters are listed in **Supplementary Table 8**.

The initial magnetization for the experiments was created in three ways: 1) using ^{1}H-^{13}C cross-polarization to preferentially detect rigid molecules, 2) using ^{1}H-^{13}C refocused INEPT to select the most mobile molecules[46], and 3) using ^{13}C direct polarization to selectively detect mobile molecules with a short recycle delay of 2 s, or to quantitatively probe all carbons and molecules with a long recycle delay of 35 s. The CP typically uses a 1 ms Hartmann-Hahn contact, with a centerband match of 50 kHz for ^{1}H and ^{13}C channels. The stepwise spectral filtration of biomolecules using the dynamical gradient was shown in **Supplementary Fig. 7**.

The narrow ^{13}C peak linewidths of 0.4-1.0 ppm allowed us to unambiguously identify the signals of major polysaccharides. To resolve and assign the ^{13}C signals of polysaccharides and proteins, 2D ^{13}C-^{13}C correlation experiments were conducted. The 2D DP refocused *J*-INADEQUATE experiment[33] correlates the double-quantum (DQ) chemical shift, the sum of the two directly bonded ^{13}C spins, with single quantum (SQ) chemical shifts. The experiment using DP, ^{13}C-^{13}C J coupling, and 1.7 s recycle delays preferentially detects mobile molecules, while the CP-based analog detects rigid molecules. The ^{13}C-^{13}C intramolecular interactions were probed using a 100 ms dipolar-assisted rotational resonance (DARR) scheme. Long-range intermolecular cross-peaks were detected using a 1.5 s proton-driven spin diffusion (PDSD) experiment. The resolved chemical shifts were compared with the values indexed in the Complex Carbohydrate Magnetic Resonance Database (CCMRD)[50], and the confirmed resonance assignments are listed in **Supplementary Table 9.**

Protein secondary structure was determined by the chemical shift differences between the observed ^{13}C chemical shifts of Cα and the standard values of random coil conformation[43]. The chemical shifts were obtained using 2D DP refocused *J*-INADEQUATE spectra for mobile amino acid residues and using 2D ^{13}C-^{13}C DARR spectra for rigid proteins.

Estimation of carbohydrate composition. The peak volumes in 2D ^{13}C-^{13}C spectra measured using 100 ms DARR and DP refocused *J*-INADEUQTAE schemes were analyzed to estimate the composition of the rigid and mobile polysaccharides, respectively (**Supplementary Table 1**). The integration function of the Bruker Topspin software was used to get the peak volumes in 2D spectra. To minimize uncertainty caused by spectral crowding, only well-resolved signals were used for compositional analysis. The NMR peaks used for quantification, their resonance assignments, and the corresponding peak volumes, were provided in Source Data file.

Solid-State NMR analysis of lipids. To probe phospholipid signals in membranes, 2D ^{1}H-^{13}C refocused INEPT spectra were collected. This experiment is based on through-bond ^{1}H-^{13}C magnetization transfer[46]. The two spin echoes contain two delays set to $1/4J_{CH}$ followed by another two delays set to $1/6J_{CH}$, which were calculated using a CH J-coupling of 140 Hz for carbohydrates. In solid samples, only the most mobile molecules with long transverse relaxation times could be observed using this experimental scheme. Therefore, the intrinsically dynamic lipids were efficiently detected. In addition, model phospholipids (POPC and POPG) were measured for comparison. Around 50 mg of samples were packed into a 4 mm rotor. 1D ^{13}C DP experiments (with a recycle delay of 3 s) and 2D ^{1}H-^{13}C refocused INEPT experiments were conducted on both model lipid samples on a 400 MHz NMR spectrometer.

Measurements of water contact and polymer dynamics. To examine the site-specific water contacts of polysaccharides and proteins, 1D and 2D water-edited ^{13}C experiments were conducted[41,42,51]. Briefly, a ^{1}H-T_2 relaxation filter (1.2 ms × 2) was used to suppress the polysaccharide signals to less than 5%, while retaining 80% of water magnetization as shown in **Supplementary Fig. 5**. The water ^{1}H polarization was then transferred to spatially proximal biomolecules through a ^{1}H-^{1}H mixing period before transferring it to carbon via a 1-ms CP for high-resolution ^{13}C detection. The ^{1}H mixing time was ranged from 0 ms to 100 ms for measuring 1D spectra and was fixed to 4 ms when the 2D spectrum was measured. Data obtained from the 1D spectra were analyzed by plotting the relative intensities as a function of the square root of the ^{1}H mixing time, which gave a buildup curve of peak intensity. The data obtained from the 2D scheme were analyzed by comparing the intensities between the water-edited spectrum (S) and the non-edited control spectrum (S_0), for each resolved carbon site. These S/S_0 intensity ratios reflect the extent of water retention around different carbon sites, which were documented in **Supplementary Tables 3** and **5** for polysaccharides and proteins.

^{13}C-T_1 relaxation was measured using CP-based Torchia T_1 scheme[52], with the z-filter duration varying from 0.1 μs to 8 s to provide complete relaxation curves as shown in **Supplementary Fig. 6**. ^{13}C-detected ^{1}H-$T_{1\rho}$ relaxation were measured using the Lee-Goldburg spin-lock sequence in which ^{1}H spin diffusion was suppressed during both the spin-lock period and the CP period to obtain site-specific ^{1}H relaxation information for protons that are directly bonded to a carbon site. A single exponential function was used to fit the data of both ^{13}C-T_1 and ^{1}H-$T_{1\rho}$ to obtain relaxation time constants, which are documented in **Supplementary Table 4**.

DATA AVAILABILITY

All relevant data that support the findings of this study are available within the article and supplementary information or upon request from the corresponding authors. The source data underlying Figs. 2a, d, and Figs. 3c-e are provided as a Source Data file.

SUPPLEMENTARY INFORMATION

Supplementary Figs. 1-10, Supplementary Tables 1-9, and Supplementary References.

ACKNOWLEGMENTS

This work was supported by the National Institutes of Health grant AI173270 to T.W. and Project-Conacyt-CB-285816 to R.A.B-G. N. G-C. acknowledge the support by the Slovenian Research Agency to Infrastructural Centre Mycosmo (MRIC UL, I0-0022) and program P4-0432. The high-field NMR spectra were collected at the Environmental Molecular Sciences Laboratory (grid.436923.9), a DOE Office of Science scientific user facility sponsored by the Department of Energy's Office of Biological and Environmental Research and located at PNNL under contract DE-AC05-76RL01830.

AUTHOR CONTRIBUTIONS

L.D.F. and L.M.A. prepared ^{13}C, ^{15}N-labeled fungal cultures. L.D.F., A.S.L., and M.D.W. conducted NMR experiments. L.D.F. and M.D.W. analyzed the NMR data. J.-P.L., R.A.B-G., N.G-C., Y.P.L., L.D.F., and T.W. interpreted the structural data. L.D.F. and M.D.W. collected the TEM images. T.W. and R.A.B-G. designed and supervised the project. All authors contributed to the manuscript writing.

COMPETING INTEREST

The authors declare no competing interests.

REFERENCES

1. Rothschild, L.J. & Mancinelli, R.L. Life in extreme environments. *Nature* **409**, 1092-1101 (2001).
2. Merino, N. et al. Living at the Extremes: Extremophiles and the Limits of Life in a Planetary Context. *Front. Microbiol.* **10**, 780 (2019).
3. Albers, S.V. Extremophiles: Life at the deep end. *Nature* **538**, 457 (2016).
4. Spang, A. et al. Complex archaea that bridge the gap between prokaryotes and eukaryotes. *Nature* **521**, 173-179 (2015).

5. van den Burg, B. Extremophiles as a source for novel enzymes. *Curr. Opin. Microbiol.* **6**, 213-218 (2003).
6. Batista-García, R.A. et al. Characterization of lignocellulolytic activities from a moderate halophile strain of Aspergillus caesiellus isolated from a sugarcane bagasse fermentation. *PLoS One* **9**, e105893 (2014).
7. Gunde-Cimerman, N., Ramos, J. & Plemenitaš, A. Halotolerant and halophilic fungi. *Mycol. Res.* **113**, 1231-1241 (2009).
8. DasSarma, S. & DasSarma, P. Halophiles and Their Enzymes: Negativity Put to Good Use. *Curr. Opin. Microbiol.* **25**, 120-126 (2015).
9. Ali, I., Khaliq, S., Sajid, S. & Akbar, A. Biotechnological applications of halophilic fungi: Past, present, and future. in *Fungi in Extreme Environments: Ecological Role and Biotechnological Significance* 291-306 (Springer, 2019).
10. Gunde-Cimerman, N., Plemenitas, A. & Oren, A. Strategies of adaptation of microorganisms of the three domains of life to high salt concentrations *FEMS Microbiol. Rev.* **42**, 353-375 (2018).
11. Kis-Papo, T. et al. Genomic adaptations of the halophilic Dead Sea filamentous fungus Eurotium rubrum. *Nat. Commun.* **5**, 3745 (2014).
12. Tafer, H., Poyntner, C., Lopandic, K., Sterflinger, K. & Pinar, G. Back to the Salt Mines: Genome and Transcriptome Comparisons of the Halophilic Fungus Aspergillus salisburgensis and Its Halotolerant Relative Aspergillus sclerotialis. *Genes* **10**, 381 (2019).
13. Zajc, J. et al. Genome and transcriptome sequencing of the halophilic fungus Wallemia ichthyophaga: haloadaptations present and absent. *BMC Genom.* **14**, 617 (2013).
14. Kogej, T. et al. Osmotic adaptation of the halophilic fungus Hortaea werneckii: role of osmolytes and melanization. *Microbiology* **153**, 4261-4273 (2007).
15. Kuncici, M.K., Kogej, T., Drobne, D. & Gunde-Cimerman, N. Morphological Response of the Halophilic Fungal Genus Wallemia to High Salinity. *App. Environ. Microbiol.* **76**, 329 - 337 (2010).
16. Pérez-Llano, Y. et al. Stress reshapes the physiological response of halophile fungi to salinity. *Cells* **9**, 525 (2020).
17. Jimenez-Gomez, I. et al. Haloadaptative Responses of Aspergillus sydowii to Extreme Water Deprivation: Morphology, Compatible Solutes, and Oxidative Stress at NaCl Saturation *J. Fungi* **6**, 316 (2020).
18. Alker, A.P., Smith, G.W. & Kim, K. Characterization of Aspergillus sydowii (Thom et Church), a fungal pathogen of Caribbean sea fan corals. *Hydrobiologia* **460**, 105-111 (2001).
19. Latgé, J.P. & Wang, T. Modern Biophysics Redefines Our Understanding of Fungal Cell Wall Structure, Complexity, and Dynamics. *mBio* **13**, Modern Biophysics Redefines Our Understanding of Fungal Cell Wall Structure, Complexity, and Dynamics (2022).
20. Ehren, H.L. et al. Characterization of the cell wall of a mushroom forming fungus at atomic resolution using solid-state NMR spectroscopy. *Cell Surf.* **6**, 100046 (2020).
21. Safeer, A. et al. Probing Cell-Surface Interactions in Fungal Cell Walls by High-Resolution 1H-Detected Solid-State NMR Spectroscopy. *Chem. Euro. J.* **29**, e202202616 (2022).

22. Kelly, J.E., Chrissian, C. & Stark, R.E. Tailoring NMR experiments for structural characterization of amorphous biological solids: A practical guide. *Solid State Nucl. Magn. Reson.* **109**, 101686 (2020).
23. Kang, X. et al. Molecular architecture of fungal cell walls revealed by solid-state NMR. *Nat. Commun.* **9**, 2747 (2018).
24. Chakraborty, A. et al. A molecular vision of fungal cell wall organization by functional genomics and solid-state NMR. *Nat. Commun.* **12**, 6346 (2021).
25. Ghassemi, N. et al. Solid-State NMR Investigations of Extracellular Matrices and Cell Walls of Algae, Bacteria, Fungi, and Plants. *Chem. Rev.* **122**, 10036–10086 (2022).
26. Fernando, L.D. et al. Solid-state NMR analysis of unlabeled fungal cell walls from Aspergillus and Candida species. *J. Struct. Biol. X* **6**, 100070 (2022).
27. Lamon, G. et al. Solid-state NMR molecular snapshots of Aspergillus fumigatus cell wall architecture during a conidial morphotype transition. *Proc. Natl. Acad. Sci. USA* **120**, e2212003120 (2022).
28. Latgé, J.-P. The cell wall: a carbohydrate armour for the fungal cell. *Mol. Microbiol.* **66**, 279-290 (2007).
29. Gow, N.A.R. & Lenardon, M.D. Architecture of the dynamic fungal cell wall. *Nat. Rev. Microbiol.* **21**, 248-259 (2022).
30. Latgé, J.P. & Chamilos, G. Aspergillus fumigatus and Aspergillosis in 2019. *Clin. Microbiol. Rev.* **33**, e00140-18 (2019).
31. Wagener, J., Striegler, K. & Wagener, N. α- and β-1,3-Glucan Synthesis and Remodeling. in *The Fungal Cell Wall: An Armour and a Weapon for Human Fungal Pathogens*, Vol. 425 (ed. Latgé, J.P.) 53-82 (Springer, Cham., 2020).
32. Gow, N.A.R., Latge, J.P. & Munro, C.A. The Fungal Cell Wall: Structure, Biosynthesis, and Function. *Microbiol. Spectr.* **5**, 1-25 (2017).
33. Lesage, A., Bardet, M. & Emsley, L. Through-bond carbon-carbon connectivities in disordered solids by NMR. *J. Am. Chem. Soc.* **188**, 10987-10993 (1999).
34. Speth, C., Rambach, G., Lass-Florl, C., Howell, P.L. & Sheppard, D.C. Galactosaminogalactan (GAG) and its multiple roles in Aspergillus pathogenesis. *Virulence* **10**, 976-983 (2019).
35. Latge, J.P. Galactofuranose containing molecules in Aspergillus fumigatus. *Med. Mycol.* **47**, S104-S109 (2009).
36. Lee, M.J. & Sheppard, D.C. Recent advances in the understanding of the Aspergillus fumigatus cell wall. *J. Microbiol.* **54**, 232-242 (2016).
37. Fernando, L.D. et al. Structural Polymorphism of Chitin and Chitosan in Fungal Cell Walls from Solid-State NMR and Principal Component Analysis. *Front. Mol. Biosci.* **8**, 727053 (2021).
38. Mauff, F.L. & Sheppard, D.C. Understanding Aspergillus fumigatus galactosaminogalactan biosynthesis: A few questions remain. *Cell Surf.* **9**, 100095 (2023).
39. Gravelat, F.N. et al. Aspergillus galactosaminogalactan mediates adherence to host constituents and conceals hyphal beta-glucan from the immune system. *PLOS Pathog.* **9**, e1003575 (2013).

40. Zhang, Y. et al. Molecular insights into the complex mechanics of plant epidermal cell walls. *Science* **372**, 706-711 (2021).
41. Ader, C. et al. Structural Rearrangements of Membrane Proteins Probed by Water-Edited Solid-State NMR Spectroscopy. *J. Am. Chem. Soc.* **131**, 170-176 (2009).
42. White, P.B., Wang, T., Park, Y.B., Cosgrove, D.J. & Hong, M. Water–Polysaccharide Interactions in the Primary Cell Wall of Arabidopsis thaliana from Polarization Transfer Solid-State NMR. *J. Am. Chem. Soc.* **136**, 10399-10409 (2014).
43. de Dios, A.C., Pearson, J.G. & Oldfield, E. Secondary and Tertiary Structural Effects on Protein NMR Chemical Shifts: an ab Initio Approach. *Science* **260**, 1491-1496 (1993).
44. Bayry, J., Aimanianda, V., Guijarro, J.I., Sunde, M. & Latgé, J.-P. Hydrophobins—Unique Fungal Proteins. *PLOS Pathog.* **8**, e1002700 (2012).
45. Plemenitaš, A. et al. Adaptation to high salt concentrations in halotolerant/halophilic fungi: a molecular perspective. *Front. Microbiol.* **5**, 199 (2014).
46. Elena, B., Lesage, A., Steuernagel, S., Böckmann, A. & Emsley, L. Proton to Carbon-13 INEPT in Solid-State NMR Spectroscopy. *J. Am. Chem. Soc.* **127**, 17296-17302 (2005).
47. Chrissian, C. et al. Solid-state NMR spectroscopy identifies three classes of lipids in Cryptococcus neoformans melanized cell walls and whole fungal cells. *J. Biol. Chem.* **295**, 15083-15096 (2020).
48. Briard, B. et al. Galactosaminogalactan activates the inflammasome to provide host protection. *Nature* **588**, 688-692 (2020).
49. Rappleye, C.A., Eissenberg, L.G. & Goldman, W.E. Histoplasma capsulatum α-(1, 3)-glucan blocks innate immune recognition by the β-glucan receptor. *Proc. Natl. Acad. Sci. USA* **104**, 1366-1370 (2007).
50. Kang, X. et al. CCMRD: a solid-state NMR database for complex carbohydrates. *J. Biomol. NMR* **74**, 239-245 (2020).
51. Lesage, A., Emsley, L., Penin, F. & Bockmann, A. Investigation of dipolar-mediated water-protein interactions in microcrystalline Crh by solid-state NMR spectroscopy. *J. Am. Chem. Soc.* **128**, 8246-8255 (2006).
52. Torchia, D.A. Measurement of proton-enhanced ^{13}C T_1 values by a method which suppresses artifacts. *J. Magn. Reson.* **30**, 613-616 (1978).